Estimation of trapped mass by in-cylinder pressure resonance in HCCI engines

José Manuel Luján[a], Carlos Guardiola[a], Benjamín Pla[a], Pau Bares[a,*]

[a] *CMT-Motores Térmicos, Universitat Politècnica de València*

Abstract

High pressure gradients at homogeneous charge compression ignition (HCCI) engines heavily excite the pressure resonance. The pressure resonant frequency depends on speed of sound in the cylinder, and thus on the bulk gas temperature. Present paper profits this relation estimating the trapped mass inside the cylinder. In contrast to other estimation methods in the literature, the presented method is based on the trace of the in-cylinder pressure during the cycle; therefore, it permits a cycle-to-cycle mass estimation, and avoids errors associated with other assumptions, such as heat transfer during compression or initial temperature of the in-cylinder gases. The proposed strategy only needs the pressure signal, a volume estimation and a composition assumption to obtain several trapped mass estimates during one cycle. These estimates can be later combined for providing an error estimate of the measurement, with the assumption of negligible blow-by. The method is demonstrated in two HCCI engines of different size, showing good performance in steady operation and presenting great potential to control transient operation.

Keywords: Trapped mass estimation, Pressure resonance, Combustion diagnosis

*Corresponding author
Email address: pabamo@etsid.upv.es (Pau Bares)

Nomenclature

CAI	Controlled auto ignition
CAD	Crank angle degrees
CFD	Computational fluid dynamics
ECU	Electronic control unit
EGR	(External) exhaust gas recirculation
EVO	Exhaust valve opening
$HCCI$	Homogeneous charge compression ignition
IGR	Internal (exhaust) gas recirculation
IVC	Intake valve closing
MFB	Mass fraction burn
OP	Operation point
$RCCI$	Reactivity controlled compression ignition
SI	Spark ignition
SNR	Signal to noise ratio
SOC	Start of combustion
$STFT$	Short time Fourier transform
TDC	Top dead center
VVT	Variable valve timing

1. Introduction

Fast combustion in automotive engines excites resonance modes of the gas mix in the cylinder, creating pressure oscillations, which become in combustion noise [1] and can seriously damage the engine. As pressure resonance plays a major role in engine knocking, it was firstly addressed for SI engines. Knocking phenomenon, consisting of spontaneous ignition of the end gas, is a major factor for efficiency limitations in spark ignition (SI) engines. C.S. Draper [2] obtained a proportional rule between the speed of sound and the resonant frequency by assuming the combustion chamber to be cylindrical. Since then, Draper's estimation has been used to locate the resonant frequency in order to avoid excessive knock in SI engines [3, 4]. Nevertheless, the cylindrical approach is not suitable for cylinders with a bowl, as has been demonstrated by Torregrosa *et al.* [5] by experimental tests and CFD studies on typical diesel engine combustion chambers.

Homogeneous charge compression ignition (HCCI) engines simultaneously present high efficiencies and low NO_x production. However, the autoignition of the mixture has two main drawbacks: the lack of a direct control of the combustion phasing, and the existence of high pressure oscillations due to rapid premixed ignition [6, 7]. Regarding the first issue, HCCI engines require combustion feedback information for the proper control of the phasing, and many authors use in-cylinder pressure signal for it [8]. In the case of HCCI engines, combustion is strongly dependent of in-cylinder charge, and a fine control of the exhaust gas recirculation, both external (EGR) and internal (IGR), is needed

for ensuring combustion feasibility. Concerning the abrupt resonance behaviour of HCCI engines, the energy delivered by resonance on this combustion modes is more concentrated on the first circumferential mode, while SI knocking resonance band is wider [9]. These reasons have encouraged the authors to find a resonance based method to detect the trapped mass in HCCI engines by using the first radial mode.

Most of the works in the literature dealing with in-cylinder pressure resonance are focused on pre-calculating the frequency from operation parameters in order to tune a band-pass filter for resonance quantification [9, 10, 11, 12, 13, 14]. The method developed in this paper inverts the process: it detects the resonant frequency in order to calculate the trapped mass, making use of the relation between the cylinder bulk temperature and the speed of sound. The method is applicable to any internal combustion engine as far as the resonance is sufficiently excited; however, the method is specially suited for HCCI engines, since the first resonance mode is strongly excited what facilitates the implementation of the method. Some precedent works have tried to use the resonance phenomenon for estimating in-cylinder variables: the first attempt was done by Hickling *et al.* [15, 16], who used the resonant frequency for estimating the bulk temperature in a heavy-duty Diesel engine; more recently, Bodisco *et al.* [17] employed a Bayesian characterization of the HCCI pressure resonance in order to simulate the resonant frequency evolution during a cycle, which is later used for inferring bulk temperature of the gas and the trapped mass.

In contrast with past works, the method developed in this paper makes use of the short-time Fourier transform (STFT) to locate the first circumferential resonance mode, it experimentally characterizes the bowl effect and makes composition assumptions in order to precisely predict the trapped mass with one cycle resolution, discarding faulty measures by detecting abnormal intra-cycles incoherence in the measurement. The method is demonstrated in two engines with HCCI combustion: controlled auto ignition (CAI), based on assisting the homogeneous combustion by a spark plug, and dual fuel reactivity controlled compression ignition (RCCI) engine, based on the control of the combustion from the mixture of two different fuels. The method has shown excellent performance in steady operation points and one cycle resolution in transient operation.

In order to explain the method in detail, the paper is organized as follows: next section introduces the basics of the pressure resonance phenomenon; following, the proposed method is presented: the procedure to detect the resonant frequency and the assumptions used to estimate the trapped mass. The main characteristics of the two HCCI engines are described in Section 4, while the results of the method on both engines are presented and discussed in Section 5. Finally, the main contributions of the method are highlighted and its possible applications are presented, with critical evaluation of its main limitations.

2. Pressure resonance

Resonance phenomenon on automotive engines consists on pressure oscillations excited by combustion. Figure 2 plots the pressure trace of a cycle where the resonance was heavily excited. Resonance behavior can be modeled by the wave equation for a continuous fluid medium in cylindrical coordinates:

$$\frac{d^2\phi}{dr^2} + \frac{1}{r}\frac{d\phi}{dr} + \frac{1}{r^2}\frac{d^2\phi}{d\theta^2} + \frac{d^2\phi}{dz^2} = \frac{1}{a^2}\frac{d^2\phi}{dt^2} \tag{1}$$

where a is the velocity of sound and ϕ is the velocity potential, namely:

$$u = -\frac{d\phi}{dx}, v = -\frac{d\phi}{dy}, u = -\frac{d\phi}{dz} \tag{2}$$

being u, v, w the velocity components in the rectangular coordinates x, y, z.

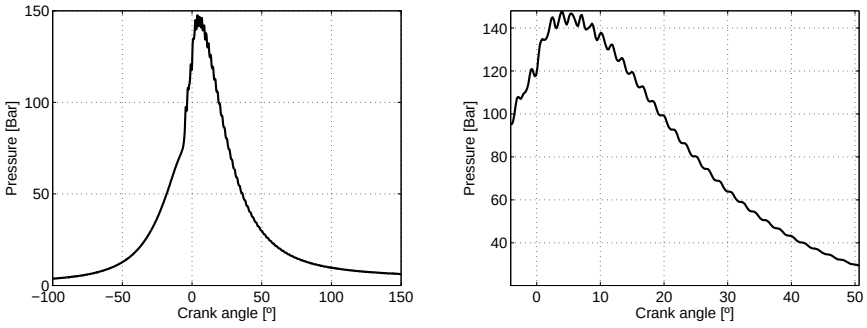

Figure 1: Pressure oscillations caused by combustion resonance in a RCCI engine at 1200 rpm and 50% load: full pressure cycle (left) and zoom over combustion (right)

The pressure waves and its resonance frequencies can be found by applying the proper boundary conditions. Despite the complex geometry in many engines combustion chambers, most works in the literature use the approach stated by Draper: solving the wave equation (1) with Bessel functions for a cylindrical geometry and obtaining a simplified solution for the different resonance modes, neglecting the axial modes ($g_k = 0$). Finally, the resonant frequency only depends on the speed of sound (a), the cylinder bore (D) and a Bessel constant ($B_{i,j}$):

$$f_{i,j} = a\sqrt{\frac{B_{i,j}^2}{(\pi D)^2} + \frac{g_k^2}{(2h)^2}} = \frac{aB_{i,j}}{\pi D} \tag{3}$$

The first circumferential and radial modes ($B_{i,j}$) are shown Figure 2.

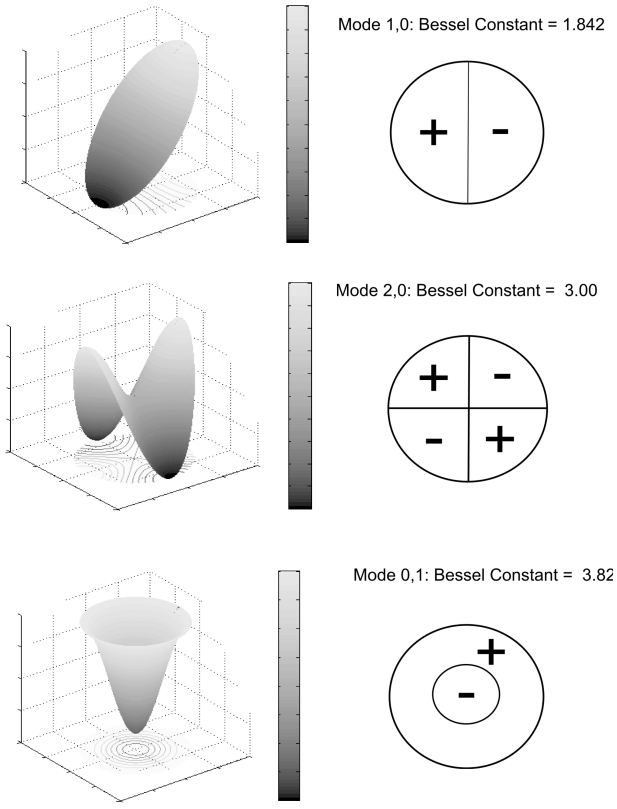

Figure 2: First circumferential and radial modes for a cylindrical chamber

Several studies verified Draper's correlation, obtaining similar experimental values for the Bessel constants, some of them were gathered in the appendix of Ref. [14]. However, two issues must be taken into account.

- Firstly, the resonance frequencies vary along a cycle, as they depend on the evolution of the speed of sound. As a result of the decrease of the gas temperature during the expansion stroke, resonant frequencies are expected to decrease. Consequently, a method with crank angle resolution may be used in order to capture the resonant frequency shift [18].
- Secondly, most automotive engines have complex bowl geometries. Chambers with bowl geometries can be assumed cylindrical far from the top dead center (TDC), nevertheless, serious discrepancies with Draper's solution exist when approaching the TDC.

Figure 3 compares the spectrogram of the pressure signal of a cycle in an actual RCCI heavy-duty engine with the theoretical solution for the first circumferential mode assuming cylindrical geometry. Although the frequency provided by the cylindrical solution (black line) almost overlaps the measured frequency (lighter part of the spectrogram, which indicates higher excitation in the pressure) when the piston is far from the TDC, Draper's solution is not valid near TDC where the chamber geometry is not cylindrical (and the bowl geometry dominates over that of the cylinder). The bowl effect over the resonance behaviour has been confirmed by experimental and CFD studies, such as [19] or [5].

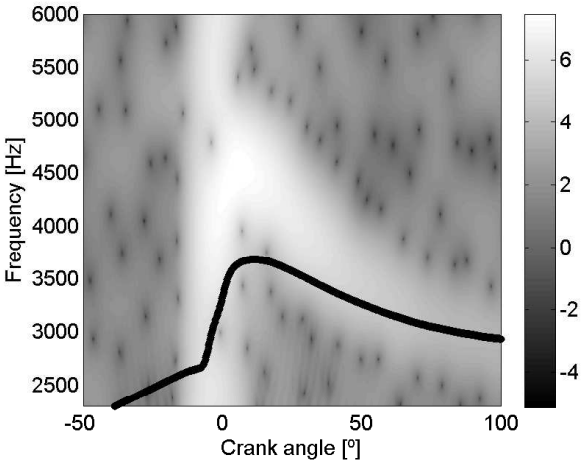

Figure 3: Spectrogram of a RCCI engine with bowl and the theoretical cylindrical resonance modes (1200 rpm, 50% load).

3. Trapped mass estimation

In-cylinder mass estimation is a recurrent topic in the literature. In research environments it is usually addressed by determining each flow separately ($\dot{m}_{air}$, $\dot{m}_{fuel}$, $\dot{m}_{EGR}$,...) by independent measurements or models [20]. The stationary uncertainty associated is quantified around 5% [21] due to the multiple sources of uncertainties, while the transient errors are considered an important problem because of the flow assumptions [22]. Other alternatives, such as volumetric efficiency equation [20], emptying-and-filling models [23, 24, 25] or Δp methods [22, 26] suffer from the simplistic approach and the use of parameters that are considered to be known and invariant with engine operation (such as volumetric efficiency, in-cylinder gas temperature, polytropic coefficient during compression, etc.).

The present method relies on the in-cylinder pressure signal, a volume estimation and a composition assumption to obtain the trapped mass. Consequently, it gravely reduces the sources of error since the assumptions are limited. Additionally, the method allows obtaining multiple measurements of the mass during a cycle, which permits deriving a metric for quantifying errors.

As previously described, HCCI engines significantly excite the first circumferential mode [9], so the method was based on the detection of this mode and its latter processing. Once the resonant frequency is identified, the following set of equations permits the mass estimation:

$$f_{1,0} = \frac{aB'_{1,0}}{\pi D} \tag{4}$$

$$m = \frac{pV}{RT} \tag{5}$$

$$a^2 = \gamma RT \tag{6}$$

Equations 4 to 6 can be combined in order to end up with:

$$m = \gamma pV \left(\frac{B'_{1,0}}{\pi D f_{1,0}} \right)^2 \tag{7}$$

where the volume can be calculated from the piston-rod-crank kinematics:

$$V(\alpha) = V_{cc} + \frac{\pi D^2}{4}[l + r\,(1 - \cos(\alpha)) - \sqrt{l^2 - r^2 \sin(\alpha)^2}] \tag{8}$$

So if the gas properties are considered constant ($\gamma = 1.3$) for a compact solution, the trapped mass is a function of the geometry and the pressure signal: pressure frequency ($f_{1,0}$) and pressure value (p).

Even though some errors can be expected from using a constant composition assumption, the composition does not significantly affect the final estimation: Appendix A bounds the maximum error associated to the composition by 4%, so a centred initial estimation limits the maximum error to $\pm 2\%$. With a sensible estimation based on the operating conditions, the effect of errors in the composition should not imply noticeable errors of the final mass calculation.

If more precision is required the gas properties (R, γ) can be obtained from experimental correlations and a composition assumption. A polynomial correlation is described in Ref. [27], by dividing the species in three groups: air, fuel and burnt products:

$$R = f(Y_a, Y_f, Y_b) \quad (9)$$

$$C_v = \frac{R}{\gamma - 1} = f(Y_a, Y_f, Y_b, T) \quad (10)$$

Concerning the composition (Y_a, Y_f, Y_b), its evolution is calculated by assuming complete combustion and employing a mass fraction burn (MFB)procedure, some of the MFB procedures are analyzed at [28]. Regarding the initial values of air, fuel and burnt products (residual gasses and recirculated gases): air mass and fuel mass are normally measured or estimated by the engine control unit (ECU), but the burnt gases are difficult to estimate accurately on board. If this configuration is considered, the system of equations defined by (4-10) can be solved by fixed point iteration or bisection following the scheme plotted in Figure 4.

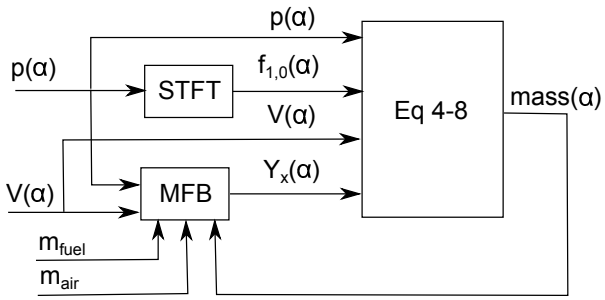

Figure 4: Trapped mass estimation through iteration

3.1. Frequency identification

Three different bands can be identified in the pressure signal spectrum of an automotive engine cycle [1]: the low frequency components (below 500 Hz) are associated with the movement of the piston, medium frequency components (between 300 Hz and 2 kHz) are related to the maximum rate of pressure rise caused by combustion [29], and punctual frequencies above 3 kHz are caused by the resonance of the chamber. The rest of the frequencies are considered noise due to the pressure sensor behaviour. It must be remarked that piezoelectric pressure sensors can also present cavity resonance, which are usually located at higher frequencies than the combustion chamber resonance (above 50 kHz).

Figure 5 shows the frequency components at two sections of the cycle shown in figures 2 and 3. Black line corresponds to a window of 50 CAD centred at -70 CAD, situated at the compression and does not take into account any combustion effect; gray line corresponds to a window centred at 20 CAD, where the effect of the combustion is apparent. For the second case, a peak at 4.5 kHz

appears, which coincides in range with the expected value for the cylindrical first mode. It must be noticed that noise (frequencies above 10 kHz) is almost the same in both zones because it is related with the sensor and acquisition chain characteristics.

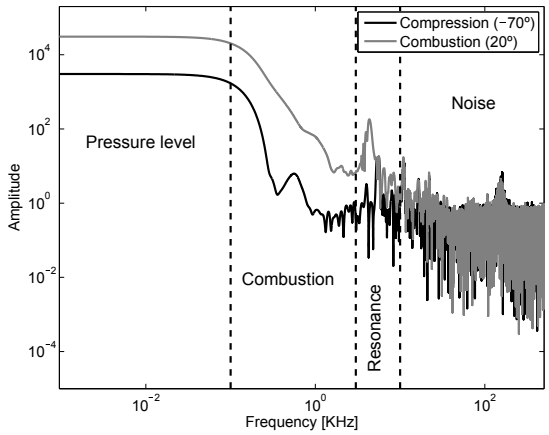

Figure 5: Pressure spectrum at compression and after ignition (RCCI combustion, 1200 rpm, 50% load)

The authors have decided to use the STFT to compute the frequency spectrum of a pressure trace since it permits obtaining a precise frequency information at different crank angles [30]. However, the location, the size and the shape of the window is crucial for a proper identification.

- Location: On one hand pressure resonance only appears after the combustion takes place, consequently, including sections of the pressure trace where there is neither combustion nor resonance that will distort the STFT. On the other hand, the resonance is damped during the expansion and low levels of resonance difficult to identify. Stanković and Böhme [31] quantified the resonance energy released in a SI engine under knocking resonance conditions, revealing that most of the resonance energy is released close to the combustion event.

  Figure 6 shows three different window locations in a HCCI cycle where the start of combustion (SOC) was located at -8^o: the first window was placed at -20^o and does not present differentiable frequency components on the resonance range, the second window, located at 20^o, presents the most preeminent resonance, and finally in the last window (centred at 60^o), although resonance is still recognizable, the peak was damped substantially.

- Size and shape: The size of the window must be sufficient to capture the

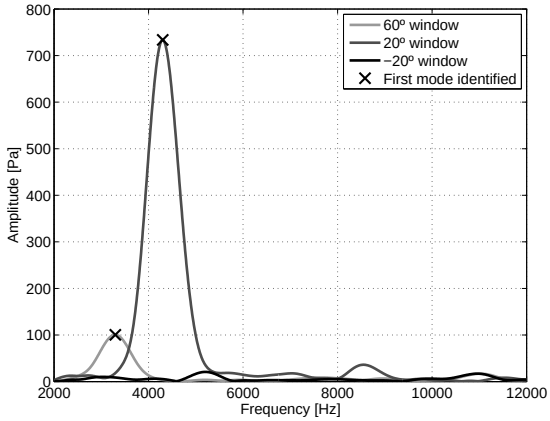

Figure 6: FFT with different window locations over the same RCCI cycle (1200 rpm, 50% load)

resonance phenomenon, but as small as possible to have sufficient crank angle resolution. The resonant frequency of the first mode depends on the geometry and the in-cylinder temperature, which vary with the crankshaft position. Using an excessive window length will result on diffusing the frequency estimation, thus providing a poor resolution. In the case of light duty engines resonance frequencies range from 5 kHz to 15 kHz, while heavy duty engines present resonant frequencies below 7 kHz; in order to capture the resonance phenomenon, the window must include at least a few periods of resonance oscillations.

The necessary size of the window is related to the window shape: a wide window shape, such as a *hamming* window, would capture the oscillations better but would also diffuse the resonant frequency. In this work, a narrow window (*Blackman-Harris*) was selected because it provides a precise location of the resonant frequency.

3.2. Bowl calibration

The problem of a non-cylindrical chamber can be faced by employing the adequate boundary conditions in equation 1, indeed this was the solution of some CFD studies over Diesel-like chambers [5]. However, complex bowl geometries are difficult to model in 3D and even then some experimental validation would be required.

The calibration proposed by the authors consists on assuming the resonant frequency proportional to the speed of sound for a given geometry, and then obtaining the proportionality at each crank angle position.

Several operation points without EGR (in order to eliminate one source of error) are selected and the trapped mass is computed by measuring the air mass flow and using models for estimating the residual gases, then the proportional constants ($B'_{i,j}(\alpha)$) can be obtained by combining equations 3 and 4 and rearranging terms, which yields to

$$B'_{i,j}(\alpha) = \frac{\pi D f_{i,j}(\alpha)\sqrt{m}}{\sqrt{\gamma(\alpha)p(\alpha)V(\alpha)}} \tag{11}$$

Figure 7 plots the experimental Bessel constants obtained at 10 operation points, run in a RCCI heavy-duty engine at 1200 rpm and at 25 %, 50 % and 75 % load: the averaged value is shown by a continuous line, while the variation obtained (average plus standard deviation) is represented by a dashed line. Two conclusion can be drawn from figure 7:

- The relation between the speed of sound and the resonant frequency varies only with the geometry, independently of the chamber conditions. Despite the high load variations (from 25% to 75%), the constants obtained for all cases were nearly identical.
- The resonance response differs a 25 % from the cylindrical solution near the top dead center, however the experimental values converge to the cylindrical solution (1.842) at the end of the stroke.

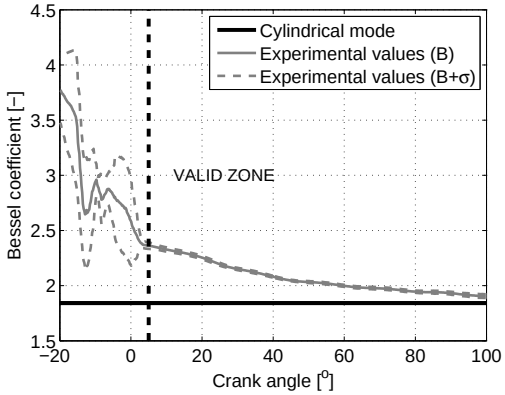

Figure 7: Experimental Bessel constants founded at 10 OP

Irregularities in the combustion chamber (whether by design, wear or manufacturing tolerance) do not gravely affect the resonance response because it is mainly characterized by the gross shape. However in order to decrease the effect of irregularities on the bowl, the method can be applied closer to the end of the stroke where they are negligible.

4. Test facilities

The pressure signal has been analyzed with a NI-PXI acquisition system composed by NI PXIe-8133 processor and different acquisition cards which allow acquiring the in-cylinder pressure both in crank angle synchronous mode (up to 0.2 CAD resolution) or time time synchronous (up to 10 MHz). The acquisition was normally crank angle based in order to have the window properly located (when using the STFT), and only few tests were recorded at 10 MHz to recognize high frequency characteristic noise (sensor cavity resonance or other resonance modes of the chamber).

For validating the method, two different engines were selected with different combustion characteristics, engine size and speed. Both were single cylinder engines and the test campaign covered significant load changes (from 25% to 100%), EGR rates and boost pressure variation for covering a significant range in the cylinder mass.

- Engine A: This engine is a four stroke, heavy duty, dual fuel engine. The phasing control was made by controlling the reactivity with two opposite fuels (RCCI) and by employing variable valve timing (VVT) [32, 33, 34]. Its geometrical size and the high pressure gradient heavily excited the resonance. For providing a reference to the in-cylinder trapped mass the following information is combined: hot-film anemometer measurement for the fresh air mass flow, a balance for the injected fuel, intake and exhaust CO_2 measurements for inferring the EGR rate, an emptying-and-filling model that computes the exhaust and intake stroke for the residuals, and an orifice model for the blow-by. The combination of all these information has an error expected to be lower than 5% for the total mass.

- Engine B: This engine is a two stroke, light duty, spark ignited engine. The engine could work as spark ignition (SI) or by controlled auto ignition (CAI) mode depending on the operation point. This engine disposed VVT which allowed controlling the air charge once the CAI mode is initiated [35, 36]. Due to the high short-circuit of the fresh air, the hardly measurable residual gases (which are bounded between 15 % to 45 % of the total trapped mass causing a significant IGR rate) and the large cyclic deviations, the mass estimations through normal procedures were expected to have large errors associated, approximately 15 %. In this case, in addition to the usual CO_2 measurement for EGR determination, CH_4 is in some cases injected in the intake manifold for providing an assessment of the short-circuit rate by measuring CH_4 concentration in the exhaust manifold.

Table 1 summarizes the main characteristics of the engines and the pressure acquisition configuration employed.

Both engines were run under constant engine speed due to the test bench limitations. However it was not due by a limitation of the method: the only

Table 1: Main engine characteristics

	Engine A	Engine B
Strokes	4	2
Combustion type	RCCI	SI/CAI
Engine speed [rpm]	1200	4000
Displacement [cc]	1806	299.8
Samples/degree	5	4
Sampling rate [kHz]	36	96
Mass error [%]	5	15
Cyclic variation	↓	↑
Resonance	↑	↓

acquisition requirement for the method is satisfying the Nyquist frequency ($F_s/2 \leq f_{1,0}$). As the pressure acquisition was crank based, the sampling rate is dependent on the engine speed and the encoder; taking into consideration the maximum resonant frequency for the engines and the encoder resolution used, the minimum allowable engine speeds were 400 rpm for Engine A and 750 rpm for Engine B, both below idle.

5. Results and discussion

For both engines, available dataset was divided into two blocks, the first used for characterizing the engine, and the second for the method assessment:

- Firstly, some operation points were selected to characterize the resonance behavior. The trapped mass (m_{trap}) was carefully calculated through a combination of sensors and models: the air mass (m_{air}) was estimated by a hot film anemometer, the EGR (m_{EGR}) was calculated by a CO_2 balance at the intake, the injected fuel mass (m_{fuel}) was sensed by a balance, the blow-by (m_{bb}) was estimated using the orifice mass principle, while the short-circuit (m_{sc}) and the residual gasses (m_{res}) were calculated by an emptying and filling model based on characterizing the valves behavior [23]. The final trapped mass was computed by the summation of each term:

$$m_{trap} = m_{air} + m_{fuel} + m_{EGR} + m_{res} - m_{bb} - m_{sc} \tag{12}$$

- Finally another set of operation points were used to test the method. Although, the set of sensors used during characterization were also employed to compare the method with reliable values, the method only makes use of the air mass flow and fuel estimations available from the ECU and a crank based pressure signal.

On all the OP tested the engine was maintained at the same engine speed and the load was varied by changing the fuel injection: from 65 mg/str to 232

mg/str on Engine A and from 4.9 mg/str to 17.6 mg/str on Engine B.

5.1. Resonance characterization

The signal to noise ratio (SNR) is a good indicator for discarding faulty measures. It compares the power of the signal with the power of the background noise: the signal in this case is the amplitude of the resonant frequency, while the noise is considered the rest of the frequency components above 2 kHz.

$$SNR = \frac{P_{signal}}{P_{noise}} = \frac{A^2_{signal}}{A^2_{noise}} \tag{13}$$

Figure 8 shows the percentage of cycles accepted for the training dataset as a function of the crank angle position of the window (STFT). Only the cycles where the resonance amplitude peak was 3 times higher than the background noise were accepted ($SNR >= 9$). The combustion and the resonance damping is different for each engine: Engine A shows easily recognizable resonance peaks after combustion, which are quickly damped in some cycles, the optimal range selected was bounded between 15 and 35 degrees after TDC. Engine B damps the resonance slowly and permits a better recognition between 40 and 60 degrees after TDC.

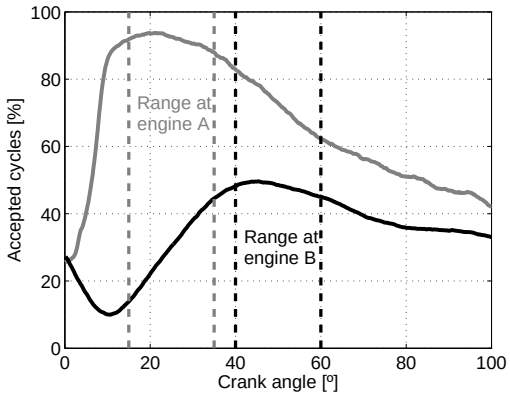

Figure 8: Percentage of accepted cycles for the SNR threshold employed

Figure 9 plots the empirical Bessel constant found by using (11) for many cycles (100 cycles per OP on Engine A and 250 cycles per OP on Engine B) over the training dataset (10 OP on Engine A and 15 OP on Engine B): the continuous line represents the reliable range selected but the dashed line was calculated from zones with poor resonance. It can be noticed that the constants extracted are slightly higher than the cylindrical constant (1.842), which is due

to the increasing importance of the bowl geometry near TDC; it may be appreciated that the calculated Bessel coefficient decreases along the expansion stroke.

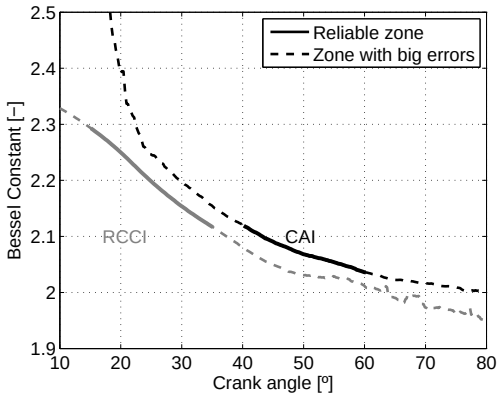

Figure 9: Bessel constants calibration for both engines: – reliable range, - - rest

5.2. Method validation

In concordance with the mass conservation principle, the mass should be nearly constant from the intake valve closing (IVC) to the exhaust valve opening (EVO), indeed the intra-cycle mass incoherences can be used to discard faulty measures. The intra-cycle error was defined as the standard deviation of the mass during the range considered, such as

$$\varepsilon = \frac{\sum_{\alpha}(m_{\alpha} - \overline{m})^2}{N_{\alpha} - 1} \tag{14}$$

Figures 10 and 11 show the estimated trapped mass during different cycles in the same operation point. The maximum intra-cycle errors plotted are 50 mg (1%) on Engine A and 3 mg (1.5%) on Engine B. The trend shown in both figures (oscillations in Engine A, and a linear decrease in Engine B), which is repeated in the different cycles shown, could be corrected through an improvement of the Bessel coefficient calibration; however, since the intra-cycle variation was below 2%, the calibration was judged to be sufficiently good.

Figures 12 and 13 plot the calculated trapped mass with their associated intra-cycle errors, for several consecutive cycles with the engine operating in steady conditions. Results show a good agreement from one cycle to the next, with the exception of a few outliers, indicating that the method permits differentiating cycle-to-cycle mass variations. This provides a better time resolution than the classical methods based on flow measurements at the intake line.

Finally, figures 14 and 15 present the comparative of the resonance method with the auxiliary method described in (12) (Black dots represent the training

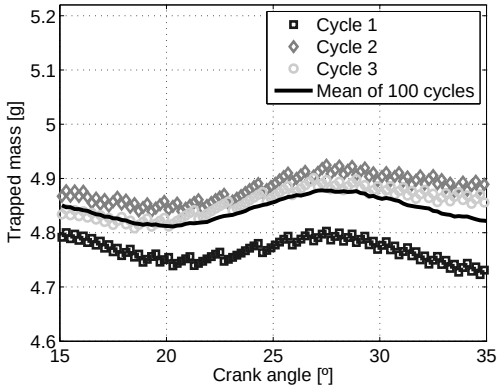

Figure 10: Calculated trapped mass over a cycle (Engine A)

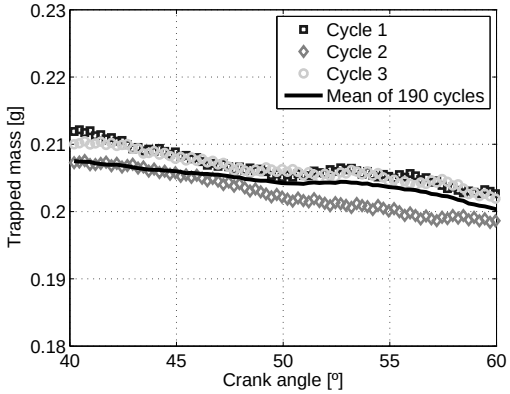

Figure 11: Calculated trapped mass over a cycle (Engine B)

dataset). The dashed line represents the expected error for both engines (higher at Engine B). The resonance method provides coherent values for almost all the tests considering the accuracy of the available methods. In the case of Engine A the divergence between the auxiliary method and the resonance based estimation is always below 5%. In the case of Engine B, the validity of the auxiliary method as reference should be questioned, as it is subject to many error sources due to the huge IGR and the existence of fresh air short-circuit. Even then, the difference between the two methods lies within the confidence region, and for the tests performed with less than 250 mg/str there is a consistent linear relationship.

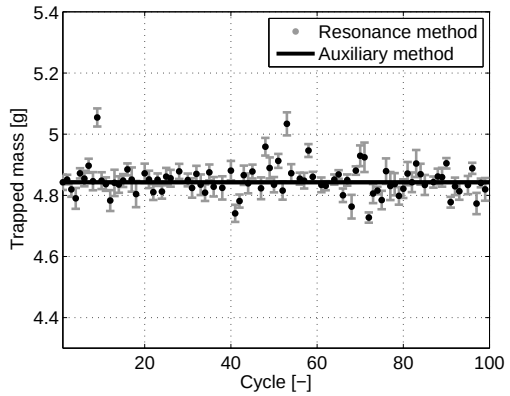

Figure 12: Calculated trapped mass for consecutive cycles measured at engine steady operation (Engine A)

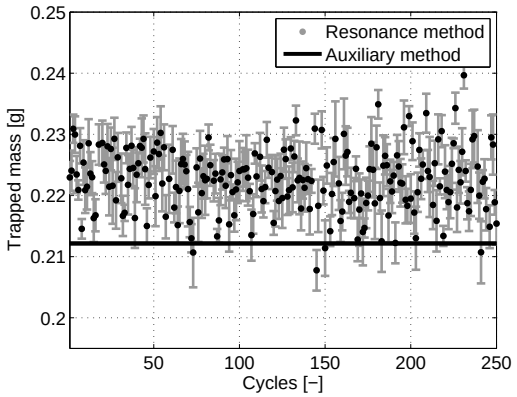

Figure 13: Calculated trapped mass for consecutive cycles measured at engine steady operation (Engine B)

6. Conclusions

A method for the estimation of the trapped mass in HCCI engines has been developed. The method is based on the resonance phenomenon of the in-cylinder pressure. Therefore, the method is free from other sources of errors, such as additional sensor measurements or adiabatic assumptions. Moreover, the utilization of the resonance offers several measurements during one cycle, which permit discarding faulty measurements. The method was tested on different engines demonstrating one cycle resolution and obtaining acceptable values when comparing with other methods.

In the authors opinion, the more important contributions of the method are:

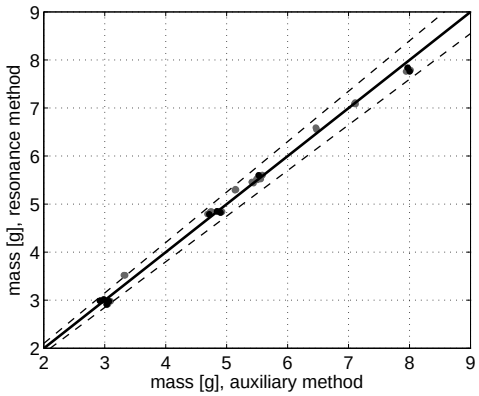

Figure 14: Calculated trapped mass over all the tested points (Engine A): – Agreement line, - - expected auxiliary method error

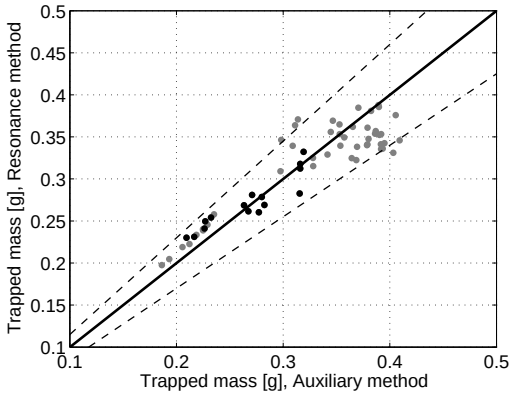

Figure 15: Calculated trapped mass over all the tested points (Engine B): – Agreement line, - - expected auxiliary method error

- Few error sources: The method permits a measurement of the trapped mass by using the pressure signal (and a hypothesis of initial composition, although it could be disregarded with limited impact). The few signals used provides a robust approach.

- One cycle resolution: The resonance of one cycle is considered independent of each combustion event, as consequence, the method developed permits one cycle resolution without using flow assumptions.

- Internal error metric: The possibility of obtaining many trapped mass values along a cycle gives an error metric based on the mass conservation principle.

For the time being, the method is currently limited to test bench diagnosis because it requires high frequency acquisition systems and ECUs with a different structure (current ECU architecture is mainly based on 2D tables, saturations and some low-level control algorithms, but it is not suitable for iterative calculations). However, the nearby implementation of the pressure sensors in commercial vehicles [37] and the advantages of the new combustion modes, make this method suitable for future automotive engines, where the trapped mass estimation can be crucial for adequate control.

Appendix A. Mass error propagation due to composition erros

The maximum error at the mass due to composition was estimated from Equation 7 by applying linear error propagation [38]:

$$\varepsilon(m) = \left|\varepsilon(\gamma)\frac{\delta m}{\delta \gamma}\right| + \left|\varepsilon(pV)\frac{\delta m}{\delta pv}\right| + \left|\varepsilon(B)\frac{\delta m}{\delta B}\right| + \left|\varepsilon(f)\frac{\delta m}{\delta f}\right| \quad \text{(A.1)}$$

$$\frac{\varepsilon(m)}{m} = \left|\frac{\varepsilon(\gamma)}{\gamma}\right| + \left|\frac{\varepsilon(pV)}{pV}\right| + 2\left|\frac{\varepsilon(B)}{B}\right| + 2\left|\frac{\varepsilon(f)}{f}\right| \quad \text{(A.2)}$$

The relative error in mass due to considering constant composition is propagated by $\varepsilon(\gamma)/\gamma$, Equations (9) and (10) are too complicated to analytically solve the problem $\varepsilon(\gamma)$, but a discrete computation by calculation of all the possible solutions is easily affordable:

$$\begin{aligned} T &\longrightarrow [500, 2500]K \\ Y_a &\longrightarrow [0, 1] \end{aligned} \quad \text{(A.3)}$$

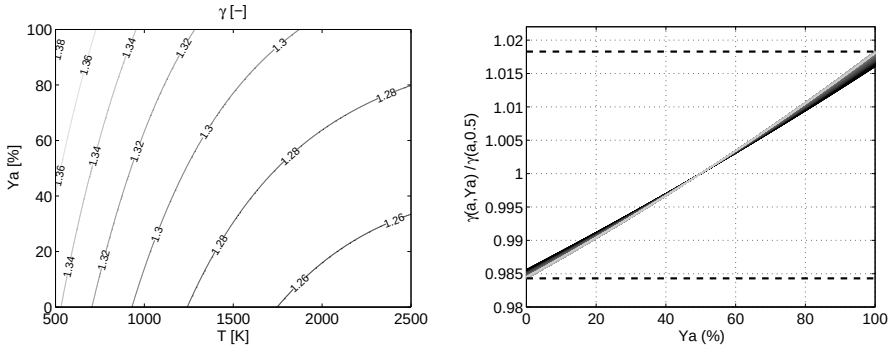

Figure A.16: γ variation due to composition: Effect of a and Y_a (left) and maximum effect due to Y_a (right)

Figure A.16 shows that with the limits stated at A.3 the mass variation is mainly due to the velocity of sound. The composition only varies the mass less than a 4% between the two possible extremes: Stoichiometric combustions (no

air) and the poorest mix (all air at the limit)[1].

[1] L. Monelletta. *Contribution to the study of combustion noise of automotive disel engines*. PhD thesis, CMT Motores Térmicos, Universidad Politécnica de Valencia, 2010.

[2] C.S. Draper. The physical effects of detonation in a closed cylindrical chamber. Technical report, National Advisory Committee for Aeronautics, 1938.

[3] X. Zhen, Y. Wang, S. Xu, Y. Zhu, C. Tao, T. Xu, and M. Song. The engine knock analysis - an overview. *Applied Energy*, 92:628–636, 2012.

[4] D. Scholl, C. Davis, S. Russ, and T. Barash. The volume acoustic modes of spark-ignited internal combustion chambers. *Society of Automotive Engineers*, 2005.

[5] A. J. Torregrosa, A. Broatch, X. Margot, V. Marant, and Y. Beauge. Combustion chamber resonances in direct injection automotive diesel engines: A numerical approach. *International Journal of Engine Research*, 5(1):83–91, 2004.

[6] X. Lu, D. Han, and Z. Huang. Fuel design and management for the control of advanced compression-ignition combustion modes. *Progress in Energy and Combustion Science*, 37(6):741–783, 2011.

[7] R. Stanglmaier and C. Roberts. Homogeneous charge compression ignition (hcci): Benefits, compromises, and future engine applications. *Society of Automotive Engineers*, 1999.

[8] J. Bengtsson, P. Strandh, R Johansson, P. Tunestål, and B. Johansson. Closed-loop combustion control of homogeneous charge compression ignition (hcci) engine dynamics. *International Journal of Adaptive Control and Signal Processing*, 18:167–179, 2004.

[9] J. A. Eng. Characterization of pressure waves in hcci combustion. *Society of Automotive Engineers*, 2002.

[10] G. Brecq, J. Bellettre, and M. Tazerout. A new indicator for knock detection in gas si engines. *International Journal of Thermal Sciences*, 42(5):523–532, 2003.

[11] G. Shu, J. Pan, and H. Wei. Analysis of onset and severity of knock in si engine based on in-cylinder pressure oscillations. *Applied Thermal Engineering*, 51(1-2):1297–1306, 2013.

[1] The fuel influence has been neglected.

[12] E. Corti and D. Moro. Knock indexes thresholds setting methodology. *Society of Automotive Engineers*, 2007.

[13] N. Cavina, E. Corti, G. Minelli, Moro D., and L. Solieri. Knock indexes normalization methodologies. *Society of Automotive Engineers*, 2005.

[14] HG. Brecq and O. Le Corre. Modeling of in-cylinder pressure oscillations under knocking conditions: Introduction to pressure envelope curve. *Society of Automotive Engineers*, 2005.

[15] Robert Hickling, Douglas A. Feldmaier, Francis H. K. Chen, and Josette S. Morel. Cavity resonances in engine combustion chambers and some applications. *Journal of the Acoustical Society of America*, 73(4):1170–1178, 1983.

[16] R Hickling, J.A. Hamburg, D.A. Feldmaier, and J.Y. Chung. Method of measuremenot of bulk temperatureso of gas in engine cylinders. *US PATENT*, 1979.

[17] T. Bodisco, R. Reeves, R. Situ, and R. Brown. Bayesian models for the determination of resonant frequencies in a di diesel engine. *Mechanical Systems and Signal Processing*, 26(1):305–314, 2012.

[18] B. Samimy and G. Rizzoni. Mechanical signature analysis using timefrequency signal processing: Application to internal combustion engine knock detection. *Proceedings of the IEEE*, 84(9):1330–1343, 1996.

[19] C. Donayre. *Estudio CFD de la resonancia en la cámara de combustión de motores diesel HDI.* PhD thesis, CMT Motores Térmicos, Universidad Politécnica de Valencia, 2013.

[20] *Internal Combustion Engine Fundamentals*. McGraw-Hill, Inc., 1988.

[21] F. Payri, S. Molina, J. Martín, and O. Armas. Inuence of measurement errors and estimated parameters on combustion diagnosis. *Applied Thermal Engineering*, 26:226–236, 2005.

[22] J. Worm. An evaluation of several methods for calculating transient trapped air mass with emphasis on the delta p approach. *Society of Automotive Engineers*, 2005.

[23] F. Payri, J. Galindo, J. Martín, and Arnau F.J. A simple model for predicting the trapped mass in a di diesel engine. *Society of Automotive Engineers*, 2007.

[24] J. W. Fox, W. K. Cheng, and Heywood J. B. A model for predicting residual gas fraction in spark-ignition engines. *Society of Automotive Engineers*, 1993.

[25] P. K. Senecal, J. Xin, and Reitz R. D. Predictions of residual gas fraction in ic engines. *Society of Automotive Engineers*, 1996.

[26] J. M. Desantes, J. Galindo, C. Guardiola, and V. Dolz. Air mass flow estimation in turbocharged diesel engines from in-cylinder pressure measurement. *Experimental Thermal and Fluid Science*, 34(1):37–47, 2010.

[27] M. Lapuerta, O. Armas, and J. J. Hernández. Diagnosis of di diesel combustion from in-cylinder pressure signal by estimation of mean thermodynamic properties of the gas. *Applied Thermal Engineering*, 19(5):513–529, 1999.

[28] M. Brunt and A. Emtage. Evaluation of burn rate routines and analysis errors. *Society of Automotive Engineers*, 1997.

[29] D. Anderton. Relation between combustion system and engine noise. *Society of Automotive Engineers*, 1979.

[30] K. Akimoto, H. Komatsu, and A. Kurauchi. Development of pattern recognition knock detection system using short-time fourier transform. In *IFAC Proceedings Volumes (IFAC-PapersOnline)*, volume 7, pages 366–371, 2013.

[31] L. Stankovi and J. F. Bhme. Time-frequency analysis of multiple resonances in combustion engine signals. *Signal Processing*, 79(1):15–28, 1999.

[32] J. Benajes, S. Molina, A. Garca, E. Belarte, and M. Vanvolsem. An investigation on rcci combustion in a heavy duty diesel engine using in-cylinder blending of diesel and gasoline fuels. *Applied Thermal Engineering*, 63(1):66–76, 2014.

[33] J. Olsson, P. Tunestål, and B. Johansson. Closed-loop control of an hcci engine. *Society of Automotive Engineers*, 2001.

[34] P. Strandh, J. Bengtsson, R. Johansson, P. Tunestål, and B. Johansson. Cycle-to-cycle control of a dual-fuel hcci engine. *Society of Automotive Engineers*, 2004.

[35] N. Jeuland and X. Montagne. New hcci/cai combustion process development: Methodology for determination of relevant fuel parameters. *Oil and Gas Science and Technology*, 61(1):85–94, 2006.

[36] N. Ravi, H. . Liao, A. F. Jungkunz, A. Widd, and J. C. Gerdes. Model predictive control of hcci using variable valve actuation and fuel injection. *Control Engineering Practice*, 20(4):421–430, 2012.

[37] J. D. Powell. Engine control using cylinder pressure: Past, present, and future. *Journal of Dynamic Systems, Measurement and Control, Transactions of the ASME*, 115(2 B):343–350, 1993.

[38] JCGM. Evaluation of measurement data - guide to the expression of uncertainty in measurement. Technical report, Joint Committee for Guides in Metrology (JCGM), 2008.